Journal of Inflammation Research

Dovepress
Taylor & Francis Group

Open Access Full Text Article

ORIGINAL RESEARCH

Obacunone Inhibits Microglia-Mediated Neuroinflammation and Ischemic Injury by Targeting Mitogen-Activated Protein Kinase 1

Jing Huang[1,2,*], Zuobin Hu[1,2,*], Jie Zhang[1,2,*], Jing Xiao[1,2], Ran Zhang[1,2], Shengnan Xia[2–5], Haiyan Yang[2–5], Xinyu Bao[2–5], Fan Zhang[6], Yun Xu[1–5], Xiaolei Zhu[1–5], Jiali Jin[1–5,7]

[1]Department of Neurology, Nanjing Drum Tower Hospital, Clinical College of Nanjing University of Chinese Medicine, Nanjing, 210008, People's Republic of China; [2]Department of Neurology, Nanjing Drum Tower Hospital, Affiliated Hospital of Medical School, Nanjing University, Nanjing, 210008, People's Republic of China; [3]State Key Laboratory of Pharmaceutical Biotechnology and Institute of Translational; Medicine for Brain Critical Diseases, Nanjing University, Nanjing, 210008, People's Republic of China; [4]Jiangsu Key Laboratory for Molecular Medicine, Medical School of Nanjing University, Nanjing, 210008, People's Republic of China; [5]Nanjing Neurology Clinical Medical Center, Nanjing, 210008, People's Republic of China; [6]State Key Laboratory of Natural Medicines and Jiangsu Provincial Key Laboratory for TCM Evaluation and Translational Research, School of Traditional Chinese Pharmacy, China Pharmaceutical University, Nanjing, 211198, People's Republic of China; [7]Department of Clinical Nutrition, Nanjing Drum Tower Hospital, Affiliated Hospital of Medical School, Nanjing University, Nanjing, 210008, People's Republic of China

*These authors contributed equally to this work

Correspondence: Xiaolei Zhu, Department of Neurology, Nanjing Drum Tower Hospital, Clinical College of Nanjing University of Chinese Medicine, 321 Zhongshan Road, Nanjing, Jiangsu, 210008, People's Republic of China, Email zhuquelee@126.com; Jiali Jin, Department of Clinical Nutrition, Nanjing Drum Tower Hospital, Affiliated Hospital of Medical School, Nanjing University, 321 Zhongshan Road, Nanjing, Jiangsu, 210008, People's Republic of China, Email jjllily@126.com

Objective: Obacunone (OB) possesses anti-inflammatory, antioxidant, and anticancer properties. This study aimed to investigate the neuroprotective effects of OB in ischemic stroke, and to elucidate the underlying mechanisms.

Methods: Primary microglia were preincubated with OB for 2 h, followed by lipopolysaccharide (LPS) stimulation for either 3 or 24 h. The levels of inflammatory cytokines in primary microglia were assessed via real-time PCR, enzyme-linked immunosorbent assay (ELISA), and Western blot. The activation of the mitogen-activated protein kinase/nuclear factor kappa B (MAPK/NF-κB) signaling pathway was evaluated via immunofluorescence staining and Western blot. For in vivo experiments, 8-week-old male C57BL/6J mice were randomly assigned to 4 groups: the sham-operated group, the middle cerebral artery occlusion (MCAO) model group and the MCAO group treated with OB (5 mg/kg/day and 10 mg/kg/day), and the sham-operated and MCAO model groups received an equivalent volume of vehicle. The neurological deficits and memory functions were evaluated by a cassette of behavior tests. 2,3,5-Triphenyl tetrazolium chloride (TTC) staining and Evans blue staining were performed to evaluate infarct size and blood-brain barrier permeability. Additionally, network pharmacology and molecular docking predicted mitogen-activated protein kinase 1 (MAPK1) as a potential target of OB, and this interaction was validated via surface plasmon resonance (SPR), cellulase thermal shift assay (CETSA), and drug affinity responsive target stability (DARTS) experiments.

Results: OB effectively inhibited the activation of the MAPK/NF-κB pathway and reduced microglia-mediated inflammatory cytokine production both in vitro and in vivo. In addition, OB attenuated ischemic brain injury in MCAO mice and improved memory function 30 days after MCAO. Moreover, OB directly bound to MAPK1, with ARG-146 as the critical binding site.

Conclusion: Our findings suggest that OB binds to MAPK1 and alleviates neuroinflammation and ischemic injury, making it a potential therapeutic agent for ischemic stroke.

Keywords: obacunone, ischemic stroke, microglia, neuroinflammation, mitogen-activated protein kinase 1

Introduction

Ischemic stroke has emerged as the third leading cause of death in China, leading to significant impairments in motor function, cognition, and overall quality of life.[1,2] This alarming statistic underscores its contribution to the national

https://doi.org/10.2147/JIR.S551466
Received: 4 July 2025
Accepted: 26 February 2026
Published: 3 March 2026

disease burden and highlights the urgent need for effective preventive strategies. Currently, the primary clinical interventions for ischemic stroke include intravenous thrombolysis and endovascular intervention. However, their effectiveness is highly time-dependent. The pathogenesis of ischemic stroke primarily involves the following mechanisms: neuroinflammation, oxidative stress, and excitotoxicity.[3] Neuroinflammation plays a pivotal role in exacerbating neuronal injury poststroke by activating immune pathways.[4] Microglia serve as central innate immune responders and are among the first cells activated during an inflammatory response following brain injury. Upon poststroke activation, microglia undergo rapid morphological changes characterized by increased cell body size and process retraction, which continuously release proinflammatory cytokines such as interleukin-1 beta (IL-1β), interleukin-6 (IL-6), tumor necrosis factor alpha (TNF-α), and reactive oxygen species (ROS).[5] A cascade of inflammatory responses leads to local tissue damage, as well as potential disturbances in distant neural circuits through systemic inflammation pathways.[6,7] Therefore, modulating microglial activation is a potential strategy for treating ischemic stroke. Our group has identified that ischemic penumbra-associated microglia (IPAMs) alleviate ischemic brain injury by producing a variety of inflammation-resolving metabolites and secreting myeloid-promoting cytokines.[8] Furthermore, we identified several chemicals, including AZD1390 and Imperatorin, that attenuate neuroinflammation and ischemic injury in MCAO mice.[9,10]

Obacunone (OB), a monomer derived from compounds extracted from citrus plants, has anti-inflammatory, analgesic, antibacterial, and antiviral properties. OB has been reported to demonstrate anti-inflammatory effects in various pathological models, including those of colitis, nonalcoholic steatohepatitis (NASH) and osteoporosis.[11–13] Notably, OB reduces glutamate-induced neurotoxicity in primary rat cortical and hippocampal neurons,[12] indicating that obacunone might be protective in neurological disorders. In this study, we revealed that OB inhibited microglia-mediated neuroinflammation and mitigated the infarct volume and memory deficits in ischemic stroke. In addition, OB directly bound to the ARG-146 site of MAPK1, and inhibit the neuroinflammation, suggesting a neuroprotective role of OB in ischemic stroke.

Materials and Methods

Reagents

Obacunone (CAS: 751-03-1, purity: 98%) was purchased from TargetMol Chemicals, Inc. (Shanghai, China), and lipopolysaccharide (LPS) was obtained from MCE (*Escherichia coli* O55:B5, USA). Obacunone was dissolved in 0.1% dimethyl sulfoxide (DMSO, Amresco, Solon, OH, USA) for in vitro experiments and in a solution of 10% DMSO, 40% PEG300, 5% Tween-80 and 45% physiological saline for in vivo studies, according to the manufacturer's instructions.

Cell Culture

Primary microglia were prepared as previously described.[14] Briefly, the cerebral cortex of newborn C57BL/6J mice was dissected and purified to isolate primary microglia. These microglia were cultured in medium consisting of 90% Dulbecco's modified Eagle's medium (DMEM) (Invitrogen, Frederick, MD, USA), 10% fetal bovine serum (FBS, HyClone, Logan, UT), and 100 U/mL antibiotics in 75 cm^2 T flasks at 37°C in a humidified environment containing 5% CO_2 for a period of 10 days. Following this incubation, the mature primary microglia were shaken gently for 3 min to facilitate suspension, after which they were seeded into 6- or 12-well plates.

Human Embryonic Kidney 293 cells (HEK-293T; ATCC, CRL-11268) and BV2 microglial cells were obtained from the China Infrastructure of Cell Line Resources (Beijing, China). The cells were maintained in medium containing 90% DMEM (Invitrogen, Frederick, MD, USA), 10% FBS (HyClone, Logan, UT), and 1% antibiotics (100 U/mL penicillin and 100 μg/mL streptomycin).

Cell Counting Kit-8 (CCK-8) Cell Viability Assay

A CCK8 (Dojindo Laboratories, Tokyo, Japan) was used to assess cell viability. Primary microglia were seeded in 96-well plates and incubated with various concentrations of OB for 24 h. Subsequently, the culture medium in each well was replaced with a mixture of the CCK8 reagent and culture medium at a 10:1 ratio. After the samples were incubated for

2–4 h, the absorbance of each well was measured at a wavelength of 450 nm via an enzyme-linked immunosorbent assay reader.

OB Treatment

For in vitro experiments, primary microglia were stimulated with LPS (100 ng/mL) to secrete inflammatory factors and were divided into the following groups: the control, LPS, and OB treatment groups (OBs: 10 μM, 25 μM and 50 μM). Primary microglia were pretreated with OB for 2 h and stimulated with LPS for 3 or 24 h.[15] For in vivo experiments, the mice were randomly divided into the following groups: the sham-operated, MCAO, and OB treatment groups. For short-term experiments, animals in the OB group received intraperitoneal injections of OB (5 or 10 mg/kg/day) for three consecutive days, whereas those in sham-operated and MCAO model groups were administered an equal volume of vehicle without OB. To evaluate long-term effects, the same dosing regimen was extended to 30 days in the OB group.

Animals and Experimental Models

Eight-week-old male C57BL/6J mice (weighing approximately 20 g) were purchased from Nanjing Gempharmatech (Nanjing, China). The animal model used in this study was reviewed and approved by Nanjing Drum Tower Hospital, Medical School of Nanjing University (approval number: 2023AE01067), performed according to the Guidelines for the Ethical Review of Laboratory Animal Welfare (GB/T 35892–2018) and the General Requirements for Laboratory Animal Experiments (GB/T 35823–2018) of the People's Republic of China. The MCAO model was constructed as follows: Mice were anesthetized with 2.5% Avertin (100–200 μL/10 g, i.p. Sigma-Aldrich). An incision was made in the middle of the neck, and the surrounding tissues were isolated. The common, external, and internal carotid arteries were examined under a microscope. A 1.5-cm-long 6-0 nylon thread plug (Docol Corporation, MA, USA) with silicone was carefully inserted from the external carotid artery into the internal carotid artery up to the beginning of the middle cerebral artery, with the plug inserted approximately 10 ± 0.5 mm to ensure proper embolization. Cerebral blood flow was monitored via a laser Doppler flowmetry device (Perimed Corporation, Stockholm, Sweden), and the plug was removed after 60 min of occlusion to restore the blood flow of the middle cerebral artery.[16] The body temperature of the mice was maintained at 37°C throughout the procedure.

The animals were randomly assigned to the sham, MCAO, or OB treatment groups via a computer-generated randomization schedule. All behavioral tests and the analyses of all outcome measures (including 2,3,5-triphenyltetrazolium chloride (TTC) staining, Evans blue quantification, and immunofluorescence) were conducted by experimenters who were blinded to the group allocation throughout the data collection and analysis phases.

Enzyme-Linked Immunosorbent Assay (ELISA)

Primary microglia were pretreated with different concentrations of OB (10, 25, and 50 μM) for 2 h and subsequently stimulated with LPS for 24 h. The supernatants were collected for ELISA analysis. Supernatants from the penumbral tissue of the mice three days after MCAO were extracted via RIPA buffer, and the resulting supernatants were obtained via centrifugation. The concentrations of IL-6, IL-1β, and TNF-α were measured via ELISA (BioWorld Biotechnology) according to the manufacturer's instructions. The absorbance (optical density, OD) was measured at 450 nm via an ELISA reader (Bio-Rad, Hercules, CA, USA).

RNA Extraction, cDNA Reverse Transcription, and Quantitative Real-Time PCR

RNA was extracted from the ischemic penumbral tissues of MCAO mice and primary microglia via the TRIzol reagent (Accurate Biotechnology, Nanjing, China). Quantitative real-time PCR (qPCR) was performed via the SYBR Green Kit (Applied Biosystems, Foster City, CA, USA). The sequences of primers used in this study were previously reported.[17,18]

Western Blot

Soluble proteins were extracted via lysis buffer (Beyotime, Shanghai, China) supplemented with protease and phosphatase inhibitors. Protein concentrations were determined via a BCA kit (Beyotime, Shanghai, China). The quantified protein samples were subsequently subjected to 10% sodium dodecyl sulfate-polyacrylamide gel electrophoresis (SDS-

PAGE) and transferred to polyvinylidene fluoride (PVDF) membranes. The membranes were then blocked with 5% skim milk and incubated overnight at 4°C, with primary antibodies targeting iNOS (rabbit, 1:1000, Cell Signaling Technology, MA, USA, Cat# 13120), COX-2 (rabbit, 1:1000, Bioworld Biotechnology, Nanjing, China, Cat# BS1076), IL-1β (rabbit, 1:1000, Cell Signaling Technology, MA, USA, Cat# 12703), TNF-α (mouse, 1:1000, Bioworld Biotechnology, Nanjing, China, Cat# BS1857), IL-6 (rabbit, 1:1000, Cell Signaling Technology, MA, USA, Cat# 12912), ERK1/2 (rabbit, 1:1000, Cell Signaling Technology, MA, USA, Cat# 4695), p-ERK1/2 (rabbit, 1:1000, Cell Signaling Technology, MA, USA, Cat# 4370), NF-κBp65 (rabbit, 1:1000, Cell Signaling Technology, MA, USA, Cat# 8242), GAPDH (rabbit, 1:5000, Bioworld Biotechnology, Nanjing, China, Cat# BS42668), and p-NF-κBp65 (rabbit, 1:1000, Cell Signaling Technology, MA, USA, Cat# 3033). The membranes were then incubated with a secondary antibody for 2 h at room temperature. The target protein bands were visualized and analyzed via the Gel-Pro system (Tanon Technologies, China), and band densities were quantified via ImageJ software (ImageJ-win 64, NIH, USA).

Immunofluorescence

After anesthesia with 2.5% Avertin, MCAO mice were subjected to cardiac perfusion with 0.1 mol/L phosphate-buffered saline (PBS) and 4% formaldehyde. Whole brains were removed, fixed overnight in 4% formaldehyde, and dehydrated in 15% and 30% sucrose solutions for 24 h. After dehydration, the brain was sectioned into 20 μm-thick slices via a cryostat and mounted onto glass slides for immunofluorescence staining. The brain sections were permeabilized with 0.25% Triton X-100 (Absin, Shanghai) and blocked with 2% bovine serum albumin (BSA) (NeoFroxx GmbH, Germany). The sections were incubated overnight at 4°C with primary antibodies against IBA1 (rabbit, 1:500; Abcam), ERK (rabbit, 1:500; CST), and NF-κBp65 (rabbit, 1:500; Abcam). The following day, after removing the primary antibodies, the corresponding secondary antibodies were applied, and the cell nuclei were stained with DAPI (Bioworld Technology, USA). Images were captured via an Olympus BX51 fluorescence microscope, and the fluorescence intensity was quantified via ImageJ software by measuring the mean gray value within regions of interest (ROIs) drawn around Iba1-positive cells or specific subcellular compartments, and microglial morphology was analyzed. The fluorescence intensity was quantified via ImageJ software. For in vitro experiments, primary microglia were cultured until adherent, treated with OB for 2 h, and stimulated with LPS for 24 h. After the supernatant was discarded, an immunofluorescence staining protocol was used.

Measurement of Infarct Volume

For infarct volume assessment, MCAO model mice were anesthetized with 2.5% avertin and euthanized via decapitation. The brains were carefully removed and sectioned into thin slices via a custom mold. The infarct areas were stained with TTC (Sigma-Aldrich) for 5–6 min. The stained slices were arranged and photographed, and the infarct volumes were quantified via ImageJ software. The infarct volume was calculated via the following formula: [(contralateral hemisphere volume − ipsilateral normal hemisphere volume)/contralateral hemisphere volume] × 100.

Blood-Brain Barrier Penetration Test

A 2% solution of Evans blue (Sigma, E2129) was injected via the tail vein at 24 and 72 h after MCAO. After 6–8 h, the limbs and skin of the mice turned blue, and the mice were anesthetized and perfused with 0.1 mol/L PBS into the heart to obtain intact brains. The brain slices were cut into 2 mm pieces and photographed. N,N-Dimethylformamide (DMF) was added to each hemisphere and the supernatant was collected by grinding and centrifugation. A 100 μL aliquot of the supernatant was added to each well of a 96-well plate, and the absorbance was measured at 620 nm via a microplate reader.

Measurement of Neurological Deficits

Behavioral tests were performed on postoperative days 1 (24 h) and 3 (72 h). The modified neurological severity score (mNSS) was used to evaluate motor, sensory, and reflex functions.[19] Grip strength was assessed via a grip strength meter (GS 3; Bioseb, France). The procedure was as follows: the mouse was gently placed on the grip dynamometer so that its forelimbs grasped the bar and then gently pulled by the tail until it released the bar. Each mouse underwent three trials,

with a 30- to 60-second rest between trials. The average of the three trials was calculated. Motor coordination and balance were assessed via a rotarod apparatus (RWD; China). Prior to testing, the mice were trained on the rotarod (set at 20, 30, and 40 rpm) for 3 consecutive days to acclimatize them to the apparatus. For the test, each mouse was placed on a rotating rod (set at 40 rpm), and the latency to fall was recorded. The foot fault test was used to assess motor coordination and limb function. The mice were placed on a horizontal grid, typically with a mesh size of 1.5 cm * 1.5 cm. During the test, the number of "foot faults" was recorded, which refers to the instances when the mouse failed to place its paw correctly on the grid and instead missed the step or stepped through the gaps. The contralateral (right) forelimb was assessed, and the total number of foot faults was counted.[20]

Open Field Test

The animal was gently placed in a designated corner of the open-field arena (40 cm × 40 cm × 15 cm), and behavioral recording commenced immediately. The animals were allowed to explore the arena freely for a duration of 10 min. Upon completion of the session, the animals were removed. The arena was thoroughly cleaned with 70% ethanol to eliminate residual olfactory cues before testing the next subject. Throughout all the procedures, the ambient lighting and acoustic conditions were held constant. The experimenter remained absent from the animal's field of view to prevent any potential influence on its behavior.[21,22]

Y Maze Test

The Y maze comprises three arms (A, B, and C; each 50 cm long, 25 cm high, and 10 cm wide) connected at 120°. Before testing, all the arms were cleaned with 70% ethanol, and arm C was blocked. The mice were habituated by free exploration of arms A and B for 15 min, and then returned to their home cage for 1 h. After the arms were recleaned and unblocked in arm C, the mice were released again and allowed to explore all three arms 20 times under video recording. Arm entry frequency and spontaneous alternations were scored. The alternation ratio was calculated as follows: (spontaneous alternations/[total entries − 2]) × 100%.

Network Pharmacology

Screening of Active Ingredients and Targets

The canonical simplified molecular-input line-entry system (SMILES) structure of the OB was retrieved from the PubChem database and imported into the SwissTargetPrediction platform (http://www.swisstargetprediction.ch/) for target prediction. The prediction parameters were set as follows: the species was selected as "Homo sapiens", and targets with a prediction probability (probability ≥ 0.1) were retained as potential therapeutic targets of OB. All prediction results were standardized for gene names using UniProt IDs as the reference.[23]

Collection of Stroke-Related Target Genes

Targets related to ischemic stroke and neuroinflammation were systematically retrieved from the following three databases: 1. GeneCards: The keywords used for retrieval, and targets with a relevance score ≥ 10 were retained; 2. OMIM: The keywords used for retrieval, followed by manual screening of genes directly related to the disease; 3. TTD: "Ischemic stroke" and "neuroinflammation" were entered into the disease search bar to obtain reported therapeutic or disease-related targets.[23] These data were merged, and duplicates were removed to construct the disease target set for ischemic stroke.

Identification of Potential Therapeutic Stroke Targets for OB

Venny mapp (https://bioinformatics.psb.ugent.be/webtools/Venn/) was used to identify gene targets related to OB and ischemic stroke, and a drug-target network was constructed via Cytoscape 3.9.1.

Protein-Protein Interactions

The list of targets was imported into the STRING database (https://string-db.org/) to construct a protein-protein interaction (PPI) network. The parameter settings were as follows: the species was set to "Homo sapiens", the minimum required interaction score was specified as "medium confidence (0.400)", and isolated nodes were hidden. The obtained

network was then imported into Cytoscape 3.9.1, and its built-in plugin CytoHubba was utilized. The targets were ranked via the "Degree"algorithm.

Gene Ontology (GO) and Kyoto Encyclopedia of Genes and Genomes (KEGG) Analyses

Gene Ontology (GO) and Kyoto Encyclopedia of Genes and Genomes (KEGG) enrichment analyses of the common targets were performed via the Genedenovo platform (https://www.omicshare.com/tools/). The GO analysis included three categories: biological process (BP), cellular component (CC), and molecular function (MF). The enrichment analysis adopted the hypergeometric distribution test, with the false discovery rate (FDR) used as the correction method and the significance threshold set at FDR < 0.05. For the KEGG pathway analysis, the same significance criterion of FDR < 0.05 was applied, and the top 20 ranked pathways were screened for visualization (bar charts and bubble charts).

Molecular Docking

The structure of the MAPK1 protein (ID: 63085) was downloaded from the UniProt database. Water molecules and the original ligand were removed via PyMOL 2.3.0. The protein structure was then imported into AutoDockTools (v1.5.6) for hydrogenation, charge calculation, and atom type assignment and saved in "pdbqt" format. POCASA 1.1 was used to predict the potential protein-binding sites, and molecular docking was performed via AutoDock Vina 1.1.2. The docking parameters were configured as follows: center_x = 22.7, center_y = 4.4, center_z = −19.6; grid box dimensions: size_x = 60, size_y = 60, size_z = 60 (grid spacing = 0.375 Å); exhaustiveness = 10; and the other parameters set to default. values. The docking results were visualized and analyzed via PyMOL 2.3.0 to evaluate the interaction modes.

Surface Plasmon Resonance (SPR)

SPR is a biophysical technique based on the principles of physical optics and is used to detect molecular interactions.[24] Briefly, the MAPK1 protein was immobilized on a CM5 sensor chip (Cytiva) via standard amine coupling chemistry to achieve a density of approximately 10,000 response units (RUs). OB was serially diluted in running buffer (10 mM HEPES, 150 mM NaCl, 0.05% v/v surfactant P20, pH 7.4, supplemented with 3% DMSO) and injected over the chip surface at a flow rate of 30 μL/min for 120 s (association phase), followed by a 180 s dissociation phase. Sensorgrams were double referenced by subtracting signals from a reference flow cell and blank buffer injections. The MAPK1 protein was immobilized on the sensor chip via an amino conjugation method, and OB was injected at increasing concentrations to bind to the MAPK1 protein. Binding and dissociation constants were determined by globally fitting the sensorgram data to a 1:1 Langmuir binding model via Biacore Insight evaluation software (Cytiva, Marlborough, MA, USA).

Drug Affinity Responsive Target Stability (DARTS)

Following 4 h of LPS stimulation, the cells were washed with PBS and lysed with NP-40 buffer on ice for 30 min. After centrifugation (12,000 × g, 10 min, 4°C), the protein concentration of the supernatant was determined via a BCA assay. The lysate was incubated with OB (50 μM) overnight at 4°C. The next day, aliquots were digested with pronase E at room temperature for 30 min. Digestion was terminated with Phenylmethylsulfonyl fluoride (PMSF), and the samples were analyzed via Western blot.[25,26]

Cellular Thermal Shift Assay (CETSA)

Primary microglia were digested with pancreatic enzymes, resuspended in 0.1 mol/L PBS, and heated at specific temperatures (37, 49, 55, 58, 61, and 64°C) for 3 min. HEK-293T cells were treated at 37, 53, 61, 69, 77 and 85°C. Following heating, the cells were subjected to three freeze-thaw cycles liquid nitrogen. The lysates were subsequently centrifuged at 13,000 rpm for 30 min at 4°C, after which the supernatants were collected as previously described.[27–29]

Plasmid Transfection

HEK-293T cells were transfected with plasmids via KeygenMAX3000 transfection reagent (KeyGEN BioTECH, Jiangsu, China). The transfection reagent mixture was prepared by adding 1 μL of transfection reagent to 25 μL of Opti-MEM®I medium (Invitrogen, Frederick, MD, USA). The DNA/enhancer mixture was prepared by adding 0.5 μg of DNA to 25 μL of Opti-MEM®I medium, followed by the addition of 1 μL of enhancer. All the components were gently mixed at room temperature to avoid vortexing or centrifugation. The DNA/enhancer mixture was combined with the

transfection reagent and incubated at room temperature for 15 min. The resulting mixture was added to the cells, and transfection was performed in an incubator at 37°C for 24–36 h before the cells were harvested for subsequent experiments. Plasmids encoding wild-type and mutant MAPK1 (R146A, R170A, and R146A/R170A double mutants) were synthesized by Nanjing Corues Biotechnology Co., Ltd. (Nanjing, Jiangsu, China).

Statistical Analysis

The experimental data were analyzed via GraphPad Prism 8.0.2 software. Data are presented as the mean ± standard error of the mean (SEM) of at least three independent biological replicates. The normality of all data were evaluated via the Shapiro–Wilk test. For comparisons among multiple groups, one-way or two-way ANOVA followed by Tukey's post hoc test was used for normally distributed data. Statistical significance was set at $p < 0.05$.

Results

OB Suppresses LPS-Induced Inflammatory Cytokine Expression in Primary Microglia

The structural formula, CAS number and SMILES of OB were shown in Figure 1A. To determine the optimal concentration range of OB for in vitro experiments, a CCK8 assay was used, and the results revealed that OB did not affect cell viability at concentrations ranging from 1–50 μM (Figure 1B).

After ischemic stroke, damaged brain cells produce many inflammatory mediators, such as platelet-activating factor, TNF-α, and IL-1β, resulting in cerebral ischemia injury.[30] To evaluate the effect of OB on neuroinflammation, we accessed the levels of proinflammatory factors in primary microglia after LPS stimulation. The results revealed that the mRNA levels of IL-1β, inducible nitric oxide synthase (iNOS), TNF-α, and IL-6 significantly increased after LPS treatment, whereas OB pretreatment reversed these effects in a dose-dependent manner (Figure 1C). In addition, the protein levels of iNOS, Cyclooxygenase-2 (COX-2), IL-1β, TNF-α, and IL-6 in microglia decreased after OB treatment (Figure 1D–H). Moreover, the levels of TNF-α and IL-6 released from primary microglia in the supernatant tended to decrease (Figure 1I and J). These results indicated that OB inhibited the expression of LPS-induced inflammatory factors in a dose-dependent manner.

OB Suppresses NF-κB Signaling Pathway in LPS-Induced Microglia

NF-κB can be rapidly induced by the inflammatory reaction after stroke and promotes the inflammatory processes of primary microglia.[31] In LPS-stimulated primary microglia, treatment with OB reduced the protein ratio of p-NF-κBp65/NF-κBp65 and suppressed the nuclear translocation of NF-κBp65 (Figure 2A–D), suggesting that OB inhibit the activation of NF-κB pathway in primary microglia following LPS stimulation.

OB Attenuates Ischemic Brain Damage in MCAO Mice

To determine whether OB alleviated ischemic brain injury and improved neurological deficits in vivo, we administered OB via intraperitoneal injection at 1, 24, and 48 h after MCAO and performed behavioral assessments (Figure 3A). The results of laser speckle contrast imaging (LSCI) revealed that cerebral blood flow was blocked in the MCAO model (Figure 3B). Injection of OB significantly reduced the infarct volume, as determined by TTC staining (Figure 3C and D). OB treatment ameliorated behavioral deficits, including improved motor function, greater grip strength, and lower mNSSs scores (Figure 3E–H). Moreover, Evans blue staining revealed decreased blood-brain barrier permeability in MCAO mice treated with OB (Figure 3I–K). Overall, OB alleviated ischemic brain injury and improved neurological deficits, suggesting that OB was a promising candidate for the treatment of ischemic stroke.

OB Attenuates Proinflammatory Cytokine Expression After MCAO

To investigate the inhibitory effects of OB on microglial inflammation after MCAO, penumbral tissue samples were analyzed. Western blot analysis revealed a trend toward decreased protein levels of COX-2 and TNF-α following OB treatment, although these changes did not reach statistical significance (Figure 4A). Quantitative real-time PCR further demonstrated that OB suppressed the mRNA expression of proinflammatory markers, including IL-6, iNOS, TNF-α, and

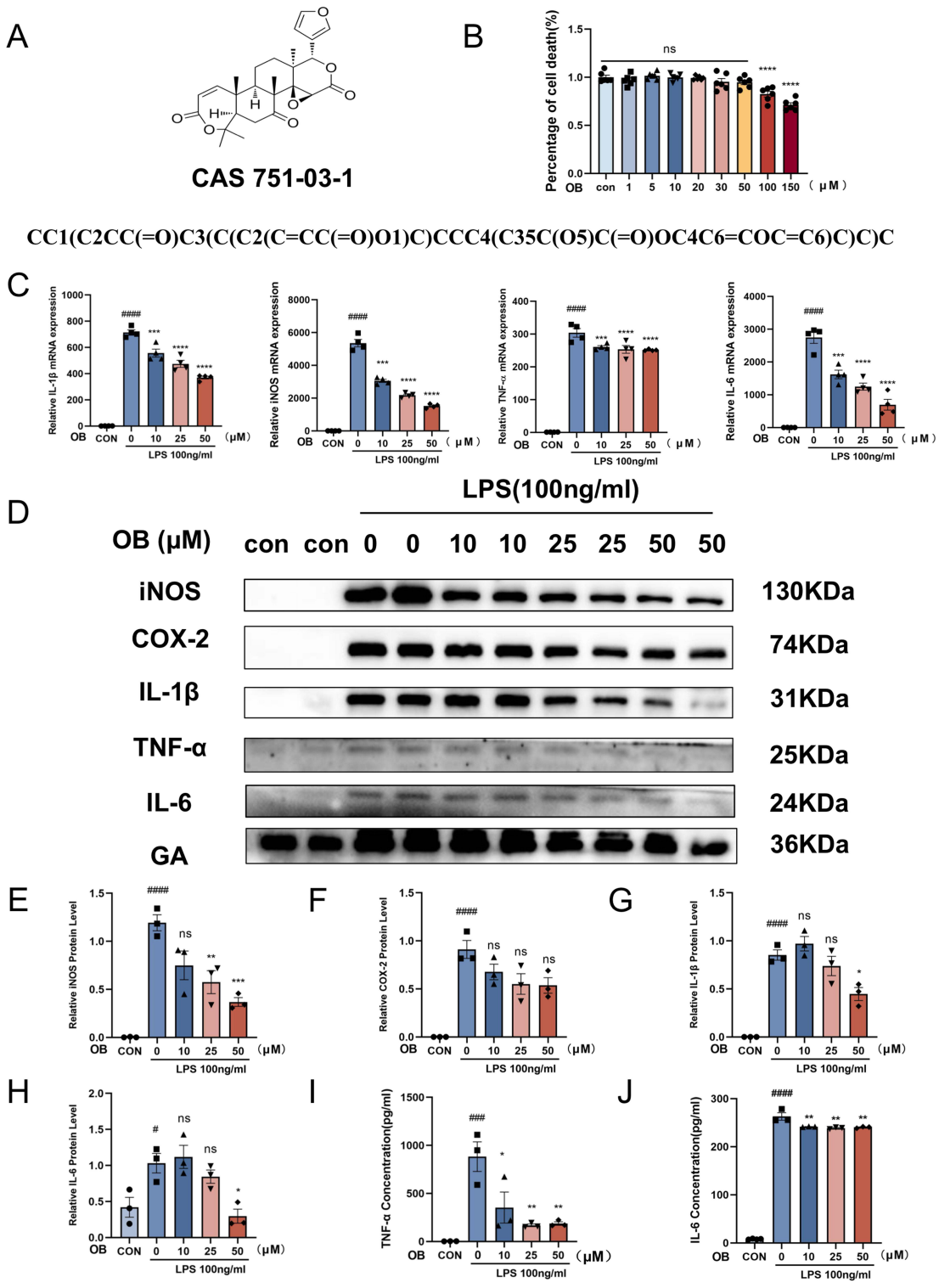

Figure 1 OB inhibited the LPS-induced expression of inflammatory factors in primary microglia. (**A**) The chemical structure, CAS number, and canonical SMILES of the OB. (**B**) Primary microglia were treated with OB at concentrations of 0, 1, 5, 10, 20, 30, 50, 100, and 150 μM for 24 h, and CCK-8 reagent was added to assess cell viability (n = 6 per group). Microglia were pretreated with different concentrations of OB (10, 25, or 50 μM) for 2 h, followed by stimulation with LPS (100 ng/mL) for 3 h or 24 h. (**C**) Following 3 h of LPS stimulation, the mRNA expression levels of IL-1β, iNOS, TNF-α, and IL-6 were measured via qPCR (n = 4 per group). (**D**) Protein levels of iNOS, COX-2, IL-1β, TNF-α, and IL-6 were assessed via Western blot after 24 h of LPS treatment, with GAPDH used as an internal control (n = 3 per group). (**E**–**H**) The gray values of iNOS, COX2, IL-1β and IL-6 in the blots were quantified via ImageJ software (n = 3 per group). (**I** and **J**) The protein levels of TNF-α and IL-6 were detected via ELISA (n = 3 per group). The different plot symbols (circles, squares, triangles, etc.) overlaid on the bar charts all indicate the sample size. The values are presented as the mean ± SEM. $^{\#}p < 0.05$, $^{\#\#\#\#}p<0.001$, $^{\#\#\#\#\#}p<0.0001$ compared with the control group; $^{*}p < 0.05$, $^{**}p < 0.01$, $^{***}p < 0.001$, $^{****}p < 0.0001$ compared to LPS-treated group.
Abbreviation: Ns, no significance.

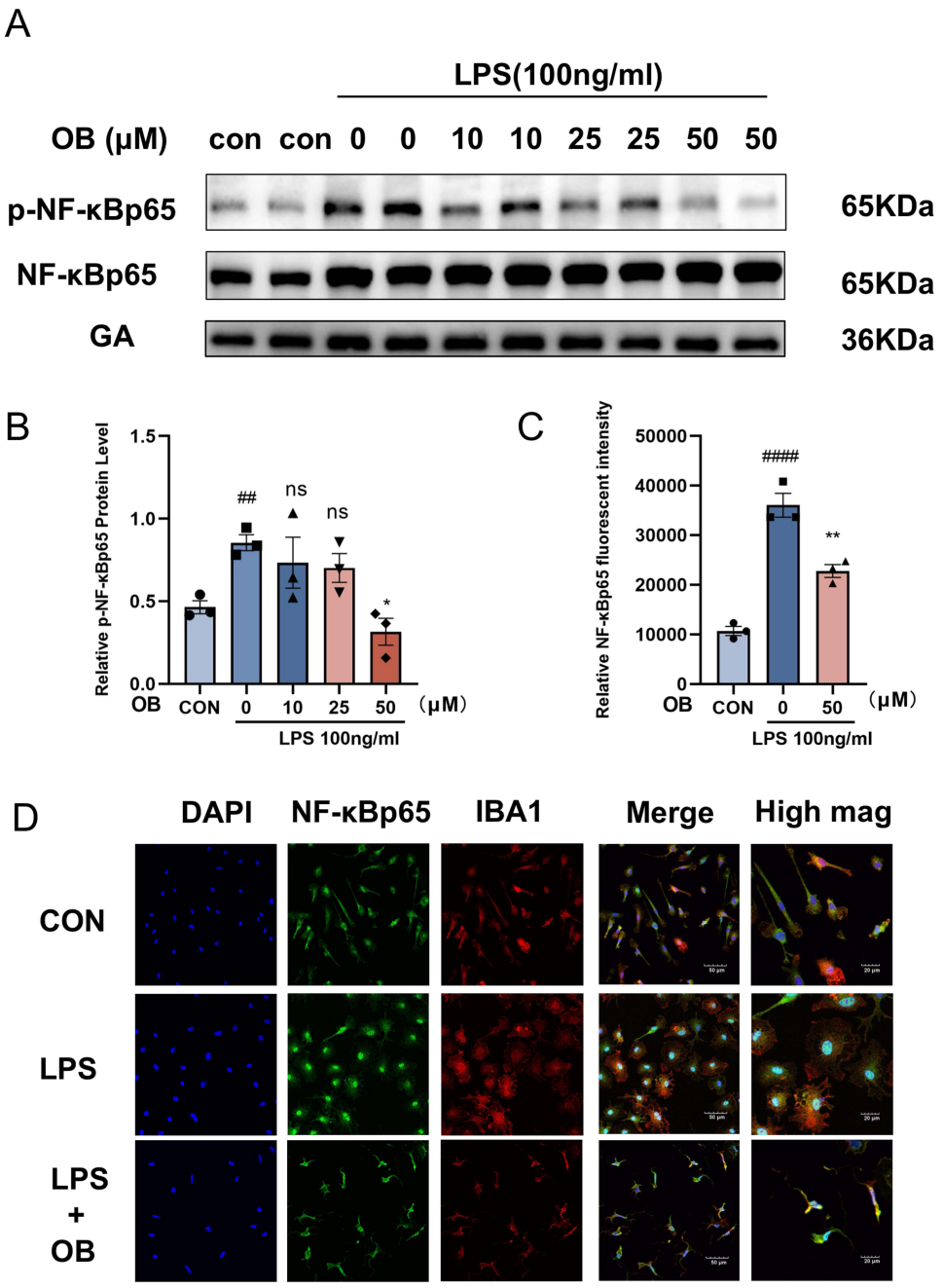

Figure 2 OB inhibited the LPS-induced NF-κB signaling pathway in microglial cells. Primary microglia were pretreated with OB (50 μM) for 2 hours, followed by LPS treatment for 24 h. (**A** and **B**) Western blot analysis was used to detect the protein levels of p-NF-κBp65/NF-κBp65 and GAPDH. ImageJ software was used to quantify the gray values of p-NF-κBp65/NF-κBp65 and GAPDH in the blots (n = 3 per group). (**C** and **D**) Immunocytochemical analysis was performed using IBA1 (red), NF-κBp65 (green) and DAPI (blue) antibodies to assess morphological changes. Scale bars: 20 μm and 50 μm. The relative NF-κBp65 fluorescence intensity was quantify with ImageJ (n = 3 per group). The different plot symbols (circles, squares, triangles, etc.) overlaid on the bar charts all indicate the sample size. The values are presented as the mean ± SEM. $^{\#\#}p < 0.01$, $^{\#\#\#\#}p<0.0001$ compared with the control group; $^{*}p < 0.05$, $^{**}p < 0.01$ compared with the LPS-treated group.
Abbreviation: Ns, no significance.

IL-1β (Figure 4B). In addition, ELISA analysis of the tissue supernatants showed significant decreases in the IL-6, IL-1β, and TNF-α levels (Figure 4C–E). Immunofluorescence-based skeleton analysis highlighted morphological changes in microglia, indicating a shift toward a less activated state. Specifically, the microglia in the OB-treated group presented smaller cell bodies, increased branching, more endpoints, and longer maximum and average branch lengths (Figure 4F–

https://doi.org/10.2147/JIR.S551466

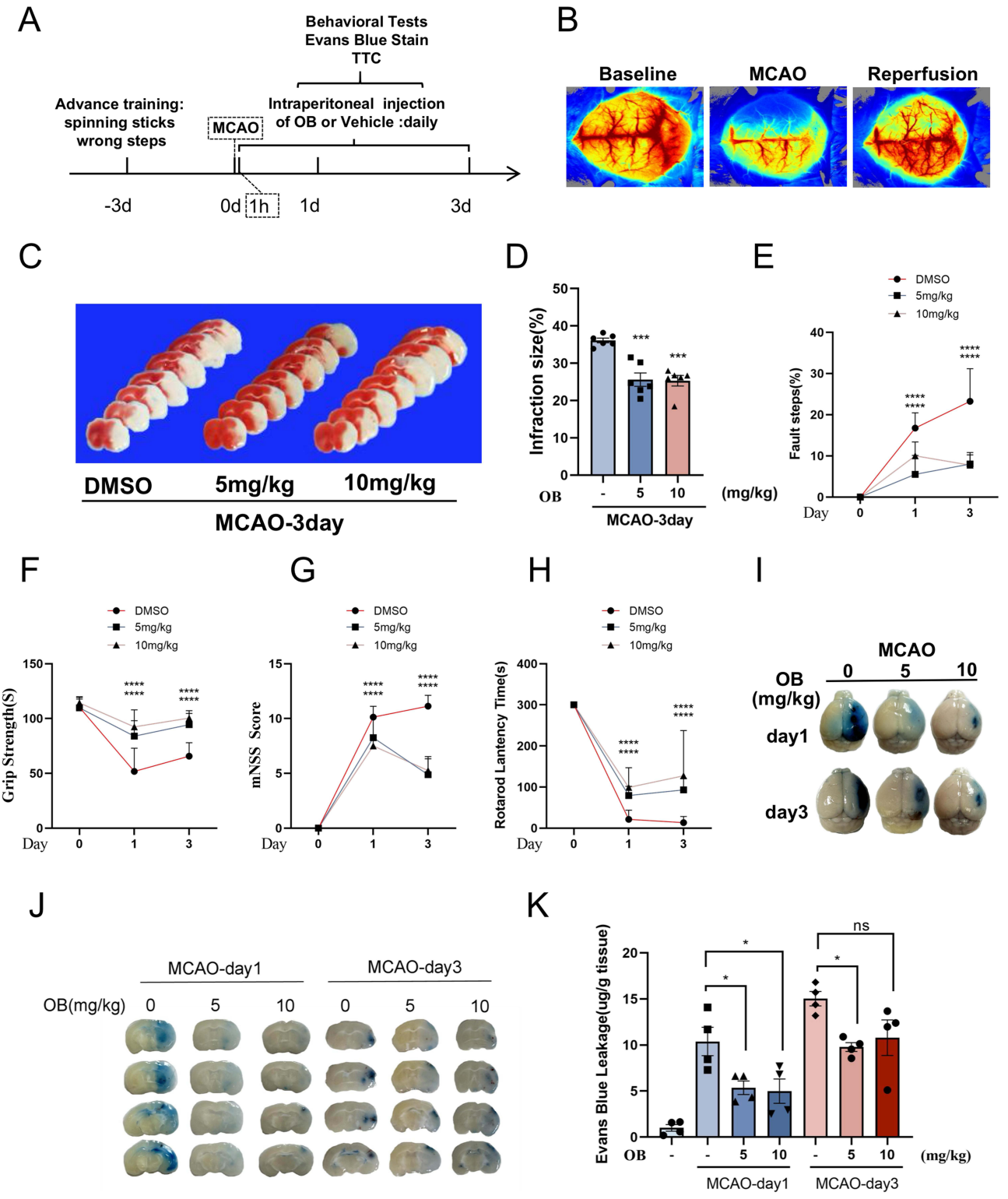

Figure 3 OB protects against ischemic brain injury and alleviates neurological deficits in MCAO mice. (**A**) Experimental timeline for short-term assessments. (**B**) LSCI maps showing cerebral blood flow before, during, and after post MCAO surgery. (**C** and **D**) Infarct size was assessed via TTC staining on day 3 after tMCAO (n = 6 mice per group). (**E**–**H**) Neurological deficits were evaluated by failure steps (**E**), grip strength (**F**), the mNSS score (**G**), and rotarod latency (**H**) at 1 and 3 days post MCAO (n = 8 mice per group). (**I**–**K**) Assessment of blood-brain barrier integrity via Evans blue extravasation. Representative images of brain hemispheres (**I**). Quantification of Evans Blue dye in the contralateral (CL) and ipsilateral (IP) hemispheres (n = 4 mice per group) (**J** and **K**). The different plot symbols (circles, squares, triangles, etc.) overlaid on the bar charts all indicate the sample size. The data are presented as the mean ± SEM. *$p < 0.05$, ***$p < 0.001$, ****$p < 0.0001$ compared with the DMSO group.
Abbreviation: Ns, no significance.

https://doi.org/10.2147/JIR.S551466

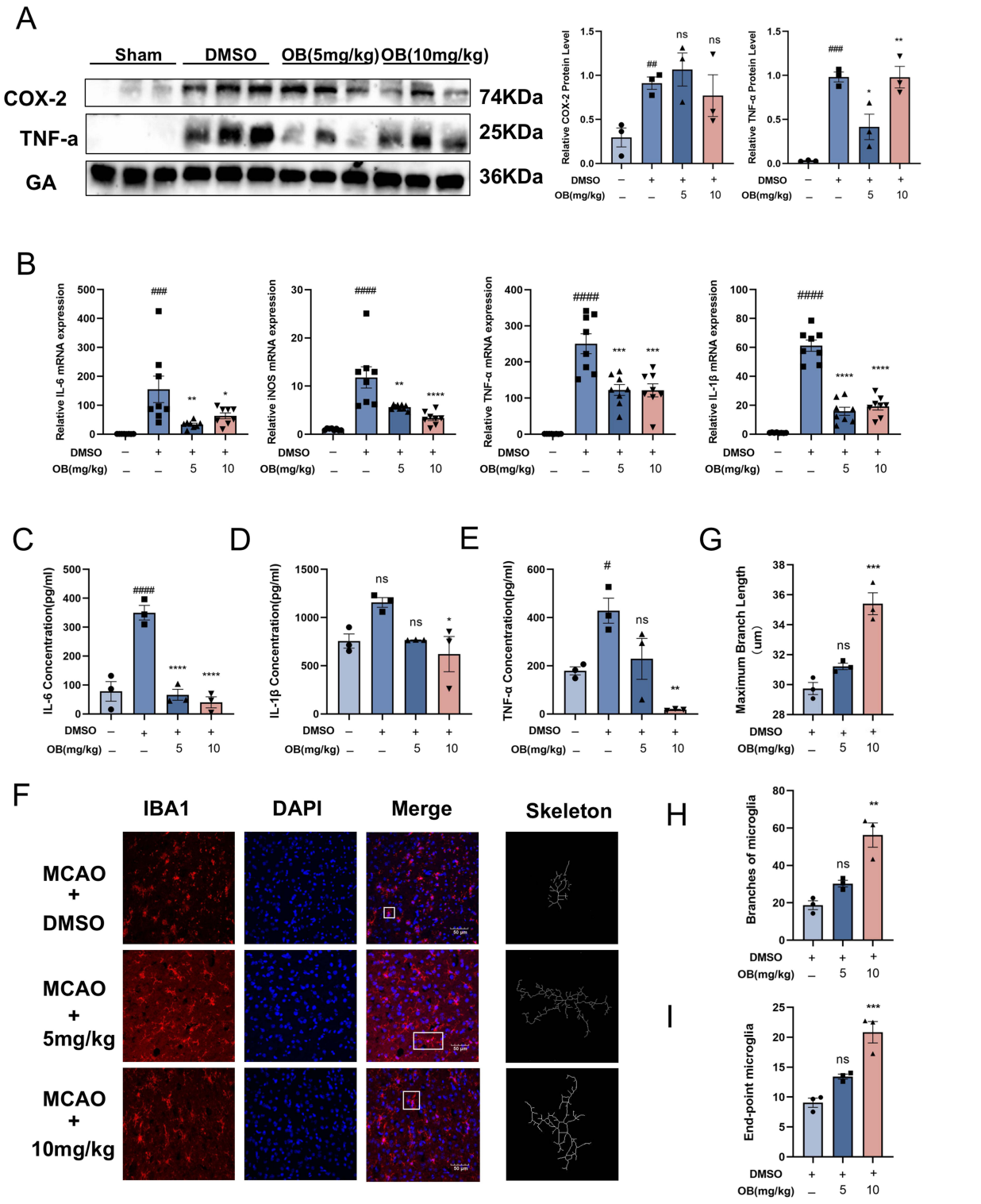

Figure 4 OB inhibited the expression of proinflammatory cytokines following ischemia. (**A**) Protein expression of COX-2 and TNF-α in the ischemic penumbra at 3 days post MCAO, as assessed by Western blot. (n = 3 mice per group). (**B**) mRNA levels of IL-6, iNOS, TNF-α, and IL-1β in ischemic penumbral tissues were quantified by qPCR (n = 8 mice per group). (**C**–**E**) Concentrations of IL-6, IL-1β, and TNF-α in protein extracts from the ischemic penumbra after MCAO were measured via ELISA (n = 3 mice per group). (**F**) Representative images of tissue sections from the ischemic penumbra of MCAO mice after 3 days, stained with IBA1 (red) and DAPI (blue). Scale bar = 50 μm. Microglial morphology was mapped. (**G**–**I**) Morphological analysis of microglia was conducted via ImageJ. The parameters assessed included the maximum branch length (**G**), microglial branch number (**H**) and endpoint count (**I**) (n = 3 per group). The white boxes indicate the regions used for high-magnification morphological mapping. The different plot symbols (circles, squares, triangles, etc.) overlaid on the bar charts all indicate the sample size. The values are expressed as the mean ± SEM. $^{\#}p < 0.05$, $^{\#\#}p < 0.01$, $^{\#\#\#}p<0.001$, $^{\#\#\#\#}p<0.0001$ compared with the sham group; $^{*}p < 0.05$, $^{**}p < 0.01$, $^{***}p < 0.001$, $^{****}p < 0.0001$ compared with the DMSO group.
Abbreviation: Ns, no significance.

https://doi.org/10.2147/JIR.S551466

I). These results suggested that the neuroprotective effect of OB might be at least partially attributed to its anti-neuroinflammatory effects.

OB Improves Long-Term Functional Recovery After Stroke

To assess the effects of OB on long-term behavioral recovery in MCAO mice, MCAO mice were treated with OB for 30 days, and then a series of behavioral tests was conducted. Consistent with the short-term treatment data, OB-treated mice presented significant improvements in sensorimotor function, including reduced foot faults, enhanced grip strength, and lower mNSSs (Figure 5A–D).

In addition, spatial memory was evaluated via open field and Y-maze tests. In the open field test, while the total distance traveled was not significantly affected among the four groups, the MCAO group spent less time exploring the central zone than the control group did, and OB treatment increased the central exploration time (Figure 5E–G). Compared with MCAO group, OB administration significantly increased the alternation rate in the Y maze

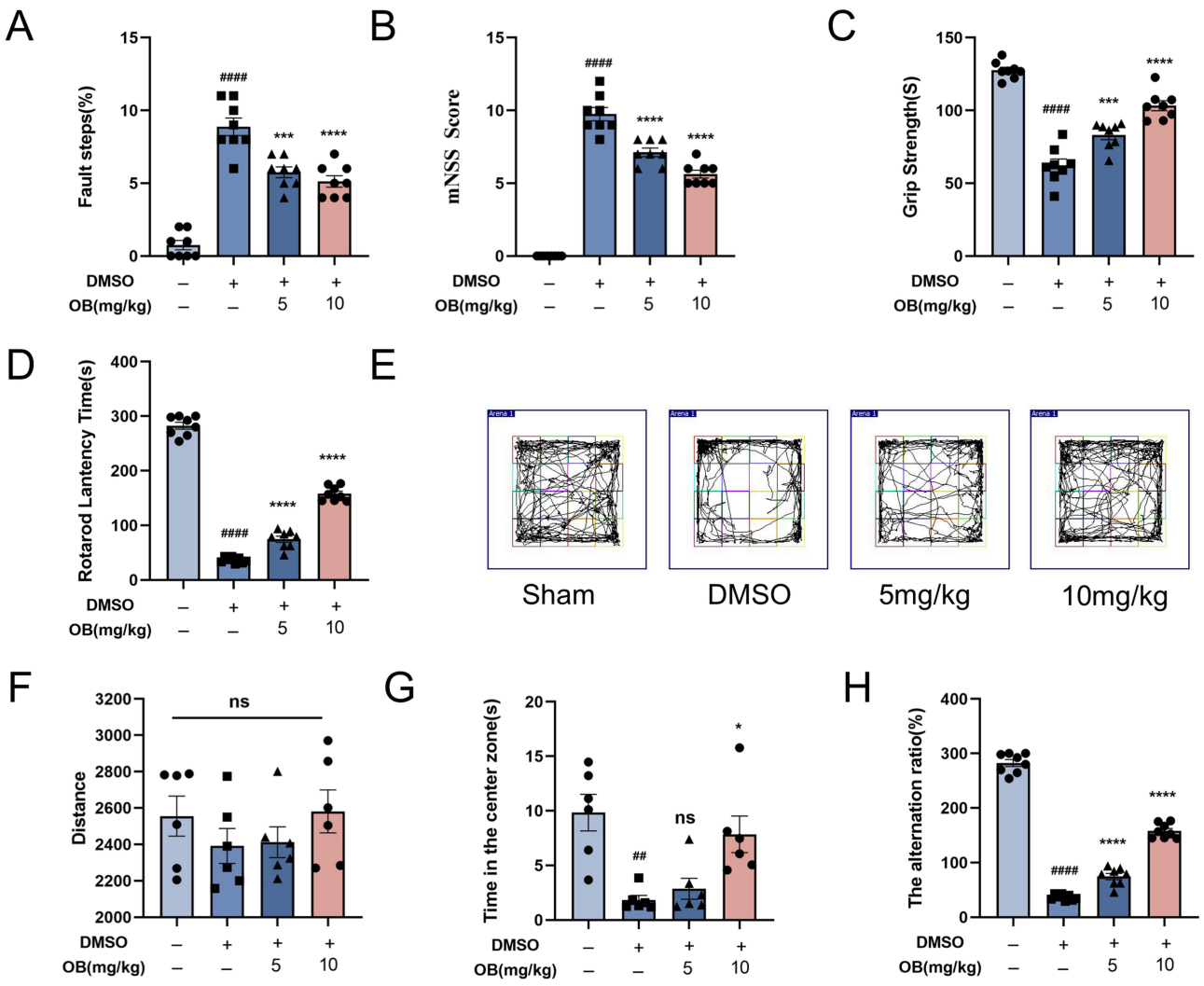

Figure 5 OB promoted long-term functional recovery in MCAO mice. (**A**–**D**) Neurological deficits were assessed by foot fault count (**A**), the mNSS score (**B**), grip strength (**C**), and rotarod lantency (**D**) (n = 8 mice per group). (**E**) Representative movement traces in the OFT. Total distance traveled (**F**) and time spent in the center zone (**G**) in the OFT (n = 6 mice per group). (**H**) Correct alternation rates in Y-maze test (n = 8 mice per group). The different plot symbols (circles, squares, triangles, etc.) overlaid on the bar charts all indicate the sample size. The values are expressed as the mean ± SEM. $^{\#\#}p < 0.01$, $^{\#\#\#\#}p<0.0001$ compared with the sham group; $^{*}p < 0.05$, $^{***}p < 0.001$, $^{****}p < 0.0001$ compared with the DMSO group.

Abbreviation: Ns, no significance.

(Figure 5H). Collectively, these results indicated that OB treatment not only improved sensorimotor function, but also promoted long-term memory functions after ischemic stroke.

Network Pharmacological Analysis[32]

Identification of OB Targets in Stroke Research

A total of 100 targets were identified via the SwissTargetPrediction software. Comprehensive searches of the GeneCards, OMIM, and TTD databases yielded 9005 stroke-related targets. Ultimately, 85 intersecting target genes relevant to the therapeutic effects of OB in stroke were identified (Figure 6A). These intersecting target genes were subsequently input into the STRING database to construct a PPI network. Network topology analysis via the degree algorithm identified 83 hub genes within the PPI network. The top four targets were as follows: *SRC* (proto-oncogene tyrosine-protein kinase Src), *CASP3* (cysteinyl aspartate-specific protease 3), *PARP1* (poly ADP-ribose polymerase-1), and *MAPK1* (mitogen-activated protein kinase 1). Although network analysis has revealed that OB may exert its effects through multiple targets, further in-depth biological validation is needed to verify its key mechanism of action. *MAPK1 (ERK2)* was selected as the focus of subsequent molecular experiments, owing to its central role in regulating cell proliferation, apoptosis and inflammatory responses, as well as its highest topological importance in the PPI network constructed in this study (Figure 6B). The compound-target interaction network diagram is shown in Figure 6C, which provides a verifiable and clear molecular entry point for the pharmacodynamic mechanism of OB.

Enrichment Analysis of Biological Functions Associated with Target Genes

Functional enrichment analysis of the GO terms revealed significant associations with OB effects (Figure 6D). KEGG pathway analysis revealed 228 pathways associated with OB in patients with stroke, with the top 20 pathways shown in Figure 6E. Notably, OB appears to regulate several crucial signaling pathways, including mitogen-activated protein kinase (MAPK) signaling, tumor necrosis factor (TNF) signaling, forkhead box O (FoxO) signaling, and the NF-κB pathway, all of which might contribute to mitigating ischemic injury.

OB Binds to MAPK1 to Inhibit the Neuroinflammatory Response

As a member of the MAPK family, MAPK1/ERK2 play a crucial role in cell growth, development, and division.[33] To assess the effects of OB treatment on MAPK1/ERK2 levels, we detected the protein expression of p-ERK1/2 both in vivo and in vitro. LPS-induced activation of the ERK pathway was significantly inhibited by OB, which was evidenced by reduced p-ERK1/2 levels (Figure 7A). OB pretreatment reduced LPS-induced ERK nuclear translocation in primary microglia (Figure 7B). Additionally, OB treatment significantly decreased p-ERK1/2 levels in the brains of MCAO mice (Figure 7C).

To explore whether OB directly binds to MAPK1/ERK2, we used two mature drug-binding techniques, CETSA and DARTS, to evaluate the affinity of the drug-target protein. CETSAs are based on the principle that drug binding stabilizes the target protein, increasing its thermal stability and reducing its degradation. DARTS operates on the basis of the principle that the binding of a small ligand to the target protein stabilizes it, thereby increasing its resistance to proteolytic enzyme hydrolysis.

In the CETSA experiment, BV2 cells pretreated with OB presented significantly greater thermal stability than those in the control group, under identical temperature conditions (Figure 8A). Compared with that of the control, the melting curve of the OB-treated group shifted significantly to the right, further confirming the stabilizing effect of OB on MAPK1 (Figure 8B). In the DARTS experiment, increasing pronase concentrations resulted in a significantly reduced degree of hydrolysis in BV2 lysates from the OB-treated group (Figure 8C). The results from both CETSA and DARTS strongly suggested a direct interaction between OB and MAPK1.

Molecular docking simulations performed via PyMOL 2.3.0 revealed that the binding energy of OB to MAPK1 was −8.68 kcal/mol, indicating high binding affinity. OB interacts with the MAPK1 protein by forming hydrogen bonds with ARG-170 (arginine-170) and ARG-146 (hydrogen bond lengths of 2.3, 2.0, 2.4, and 2.4 Å). OB formed hydrophobic interactions with THR-61 (threonine-61), GLN-60 (glutamine-60), GLN-64 (glutamine-64), LEU-33 (leucine-33), LYS-201 (lysine-201), TYR-185 (tyrosine-185), and VAL-186 (valine-186) (Figure 8D). To further validate these findings,

 https://doi.org/10.2147/JIR.S551466

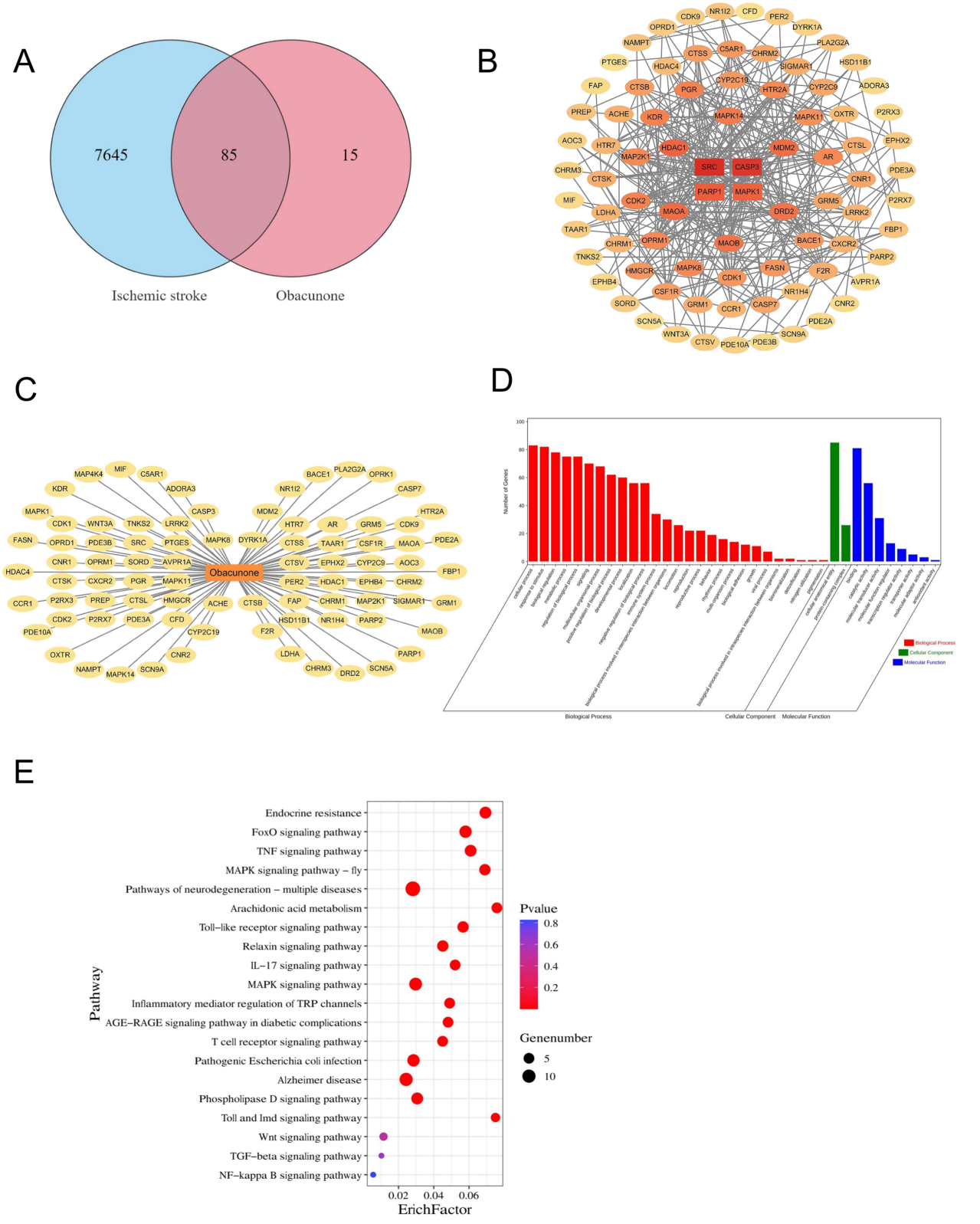

Figure 6 Pharmacological analysis of therapeutic target networks for stroke and OB, as well as functional enrichment of target genes and core signaling pathways. (**A**) OB-stroke interacting genes. (**B**) Compound-target network diagram. (**C**) PPI network of OB in stroke. (**D**) GO enrichment analysis. (**E**) The top 20 signaling pathways identified by KEGG pathway enrichment analysis.

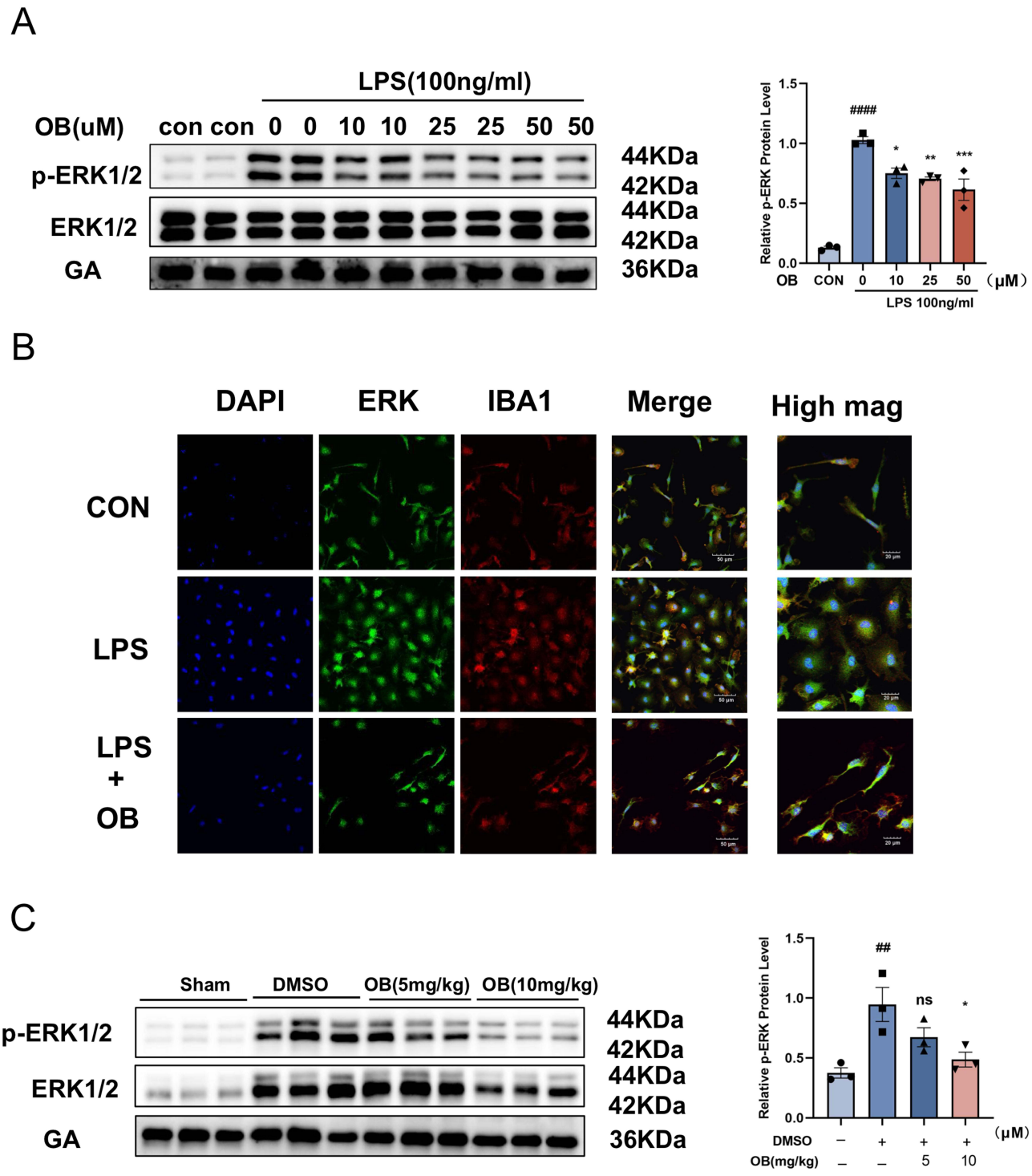

Figure 7 OB inhibits p-ERK1/2 expression in vitro and in vivo. (**A**) p-ERK1/2 expression in primary microglia decreased after OB treatment (n = 3 per group). (**B**) LPS-stimulated primary microglia, OB (50 μM) pretreatment reduced LPS-induced ERK nuclear translocation in primary microglia. DAPI (blue), ERK (green), and IBA1 (red). Scale bar = 50 μM. (**C**) OB treatment reduced p-ERK1/2 expression in penumbral tissue. The gray values of p-ERK1/2 in the blots were calculated via ImageJ software (n = 3 mice per group). The different plot symbols (circles, squares, triangles, etc.) overlaid on the bar charts all indicate the sample size. The values are presented as the mean ± SEM. $^{\#\#}p < 0.01$, $^{\#\#\#\#}p<0.0001$ compared with the sham group; $^{*}p < 0.05$, $^{**}p < 0.01$, $^{***}p < 0.001$ compared with the DMSO group.
Abbreviation: Ns, no significance.

https://doi.org/10.2147/JIR.S551466

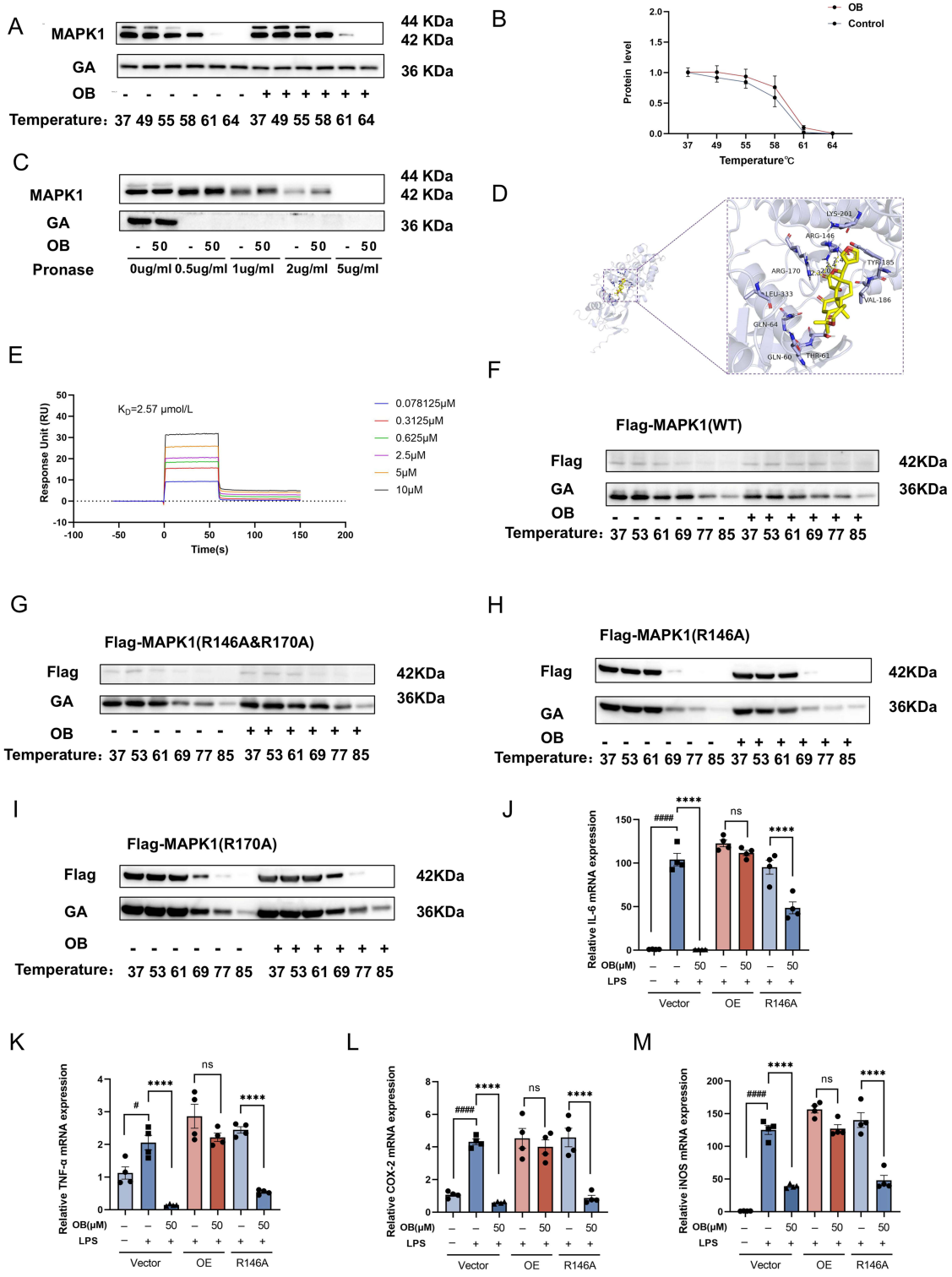

Figure 8 OB interacts with MAPK1 ARG-146 and inhibits neuroinflammation. (**A**) MAPK1 expression in OB-pretreated and untreated BV2 samples was assessed via CETSA. (**B**) A dissolution curve was generated to illustrate variations in the target protein content at different temperatures. (**C**) MAPK1 expression levels were evaluated through DARTS experiments. (**D**) Molecular docking of OB with MAPK1 was conducted via AutoDockTools software. (**E**) SPR analysis was performed to assess OB binding (0–10 μM) to immobilized MAPK1, and the equilibrium dissociation constant were obtained. (**F–I**) In the CETSA, HEK-293T cells were transfected, and the cells were incubated at various temperatures. Western blot was used to detect the binding of MAPK1 in OB-pretreated and untreated samples. (**J–M**) The mRNA levels of IL-6, TNF-α, COX-2 and iNOS in BV2 cells were quantified via qPCR (n = 4 per group). The different plot symbols (circles, squares, triangles, etc.) overlaid on the bar charts all indicate the sample size. The values are expressed as the mean ± SEM. $^{\#}p < 0.05$, $^{\#\#\#\#}p<0.0001$ compared with the control group; $^{****}p < 0.0001$ compared with the LPS-treated group.

Abbreviation: Ns, no significance.

SPR analysis was conducted to assess the affinity between OB and purified MAPK1 protein. SPR analysis confirmed a high-affinity interaction, with an equilibrium dissociation constant (K_D) of 2.57 μmol/L (Figure 8E).

To further elucidate the mechanism of binding between OB and MAPK1, CETSA experiments were conducted using plasmids encoding wild-type MAPK1 and its mutant variants (R146A, R170A, and R146A/R170A). In HEK-293T cells, OB treatment increased the thermostability of wild-type MAPK1 (Figure 8F), whereas the double mutant had the opposite effect (Figure 8G). These results indicated that ARG-146 and ARG-170 are critical sites for OB binding to MAPK1. Notably, MAPK1 was not protected by OB following mutation of ARG-146, whereas the thermostability of the R170A mutant was increased (Figure 8H and I).

To validate the critical role of ARG-146 of MAPK1 in the anti-neuroinflammatory effects of OB, we transfected BV2 cells with plasmids overexpressing wild-type or R146A mutant MAPK1 followed by OB and LPS treatment. OB treatment significantly decreased the mRNA levels of IL-6, TNF-α, COX-2, and iNOS induced by LPS, which was abolished by wild-type MAPK1 overexpression. However, R146A mutant MAPK1 overexpression did not affect the anti-neuroinflammatory effects of OB, indicating that ARG-146 is a key biological functional site for the OB-MAPK1 interaction (Figure 8J–M). Collectively, these results provide strong evidence that OB interacts with ARG-146 of MAPK1 to inhibit neuroinflammation in ischemic stroke.

Discussion

Our study demonstrated the anti-inflammatory and neuroprotective effects of OB and explored the underlying mechanisms. OB suppressed microglial activation, reduced the release of proinflammatory factors, and improved behavioral deficits in mice subjected to MCAO. Mechanistically, we found that OB directly bound to MAPK1/ERK2 and identified ARG-146 as the critical binding site. In conclusion, these data provided a promising therapeutic strategy to target neuroinflammation in ischemic stroke.

The immune system plays a crucial role in maintaining brain homeostasis. As essential immune cells in the central nervous system, microglia respond first to neuroinflammation during stroke.[34] Activated microglia release a series of proinflammatory cytokines and chemokines, which induce neuronal damage and exacerbate brain injury.[35] Increasing evidence suggests that microglia-mediated neuroinflammation plays a pivotal role in ischemic stroke.[36] OB is a monomeric compound extracted from natural plants that has been confirmed to have anti-inflammatory, antitumor, antiviral, and neuroprotective effects. OB has been shown to delay abnormal cell proliferation and cyst expansion in the treatment of autosomal dominant polycystic kidney disease.[37] In an acute lung injury model, OB inhibits the ubiquitin-proteasomal degradation of Nrf2, and blocks lipopolysaccharide-induced ferroptosis.[38] OB also modulates sphingolipid pathways to suppress NLRP3 inflammasome activation and exert anti-inflammatory effects.[39] Additionally, OB can regulate the gut microbiota and restore intestinal epithelial barrier integrity to suppress dextran sulfate sodium (DSS)-induced ulcerative colitis.[40] As one of the methanol extracts from the root bark of Dictamnus dasycarpus, OB suppressed microglial activation, reduced the release of proinflammatory cytokines, and subsequently improved functional outcomes in MCAO model mice, making it a potential candidate for the treatment of stroke. Notably, clinical treatments for ischemic stroke include intravenous thrombolysis, endovascular thrombectomy, and antiplatelet/ anticoagulants treatments,[41] and there have been no preventative drugs. To better simulate the clinical situation, OB was intraperitoneally injected at 1, 24, and 48 h after MCAO, and further investigation of the potential preventative effects of OB will be performed in the following studies.

To further explore the therapeutic mechanism of OB, we performed network pharmacology predictions and molecular docking analyses, and identified MAPK1/ERK2 as the most promising target. When phosphorylated, ERK translocates to the nucleus to regulate transcription factor activity and exerts anti-inflammatory effects. Previous studies have highlighted the neuroprotective role of the inhibition of the MAPK/ERK pathway in ischemia-reperfusion injury. Clemastine improves oligodendrocyte proliferation and exerts neuroprotective effects by inhibiting the MAPK/ERK pathway.[42] Exogenous 17β-estradiol (E2) inhibits the MAPK/ERK1/2 signaling pathway and decreases the levels of p-ERK1/2 in the ischemic hemisphere.[43] Overexpression of $ERK2^{WT}$ induces severe injury after MCAO, reduces blood-brain barrier integrity, and exacerbates infarct size and neurological deficits.[44] Pfaffia paniculata reduces intestinal inflammation by regulating the expression of MAPK and mucin genes.[45] In a cuprizone-induced demyelination mouse model, ERK2

activation in astrocytes causes inflammation.[46] These results suggest that the MAPK/ERK signaling pathway plays a crucial role in ischemia-reperfusion injury following stroke. In this study, OB inhibited the activation of the MAPK/ERK pathway and reduced the expression of inflammation-related cytokines. Moreover, OB bound to the ARG-146 site of MAPK1, which contributed to its neuroprotective effects in MCAO mice. However, further studies using *MAPK1* knockout mice are needed.

NF-κB is a classic proinflammatory signaling pathway, and inhibition of the NF-κB pathway is a promising strategy for treating ischemic stroke.[47] Interestingly, NF-κB has been shown to be a downstream target of MAPK1. The MAPK pathway, particularly the ERK pathway, can act as an upstream regulator of NF-κB activation. The phosphorylation of IκB by IKK, which is itself regulated by upstream kinases, including those in the MAPK pathway, leads to IκB degradation and the subsequent nuclear translocation of NF-κB to initiate proinflammatory gene transcription.[48–50] Kaempferol attenuates microglia-mediated neuroinflammation through the inhibition of the MAPK-NF-κB signaling pathway.[51] In macrophages, endogenous activation of the TLR2-MAPK-NF-κB axis drives the production of proinflammatory mediators.[52] Ginsenoside compound K inhibits inflammation and lipid accumulation in macrophages by downregulating the MAPK and NF-κB signaling pathways.[53] In this study, we found that the R146A mutation at least partially abolished the anti-inflammatory effect of OB. ARG-146 is located in the kinase's active site, a region crucial for substrate recognition and catalytic activity, and OB binding at this site likely interferes with the ability of MAPK1 to phosphorylate its downstream targets, including those involved in the activation of NF-κB. However, further experiments are needed to elucidate the interactions of these pathways.

While this study provides evidence for the neuroprotective effects of OB in ischemic stroke, several limitations should be acknowledged. First, the absence of a positive control group (eg, nimodipine or another established neuroprotectant) limits direct comparison of OB efficacy with that of current therapeutic drugs. Second, the therapeutic potential of OB was evaluated in 8-week-old male C57BL/6J mice. Since stroke is predominantly a disease of order people and is frequently accompanied by comorbidities such as hypertension and diabetes, the efficacy and safety of OB remain to be validated in aged and female animals. Third, OB was used after the MCAO model in the in vivo experiments, and whether OB pre-treatment protects against ischemic stroke needs further investigation.

Conclusions

In this study, we have shown that OB reduces microglia-mediated neuroinflammation in vitro and in vivo, and alleviates ischemic injury in MACO mice. OB directly binds to ARG-146 on MAPK1 and downregulates the NF-κB pathway, making it a potential lead chemical for the treatment of ischemic stroke.

Data Sharing Statement

The data will be made available upon reasonable request from the corresponding authors, Dr. Xiaolei Zhu and Dr. Jiali Jin.

Ethics Approval Statement

This study was conducted in accordance with the ethical standards of the Institutional Ethics Committee, and the animal model used in this study was reviewed and approved by Nanjing Drum Tower Hospital, Medical School of Nanjing University (Animal Ethics approval number: 2023AE01067). All procedures were performed following: the Guidelines for the Ethical Review of Laboratory Animal Welfare (GB/T 35892-2018) and the General Requirements for Laboratory Animal Experiments (GB/T 35823-2018) of the People's Republic of China.

Acknowledgments

We express our sincere thanks to all the individuals and organizations who contributed to this study. Special thanks go to Drum Tower Hospital for providing the necessary laboratory equipment and resources.

Author Contributions

All authors made a significant contribution to the work reported, whether in the conception, study design, execution, acquisition of data, analysis, and interpretation, or in all these areas, took part in drafting, revising, or critically reviewing the article; gave final approval of the version to be published; agreed on the journal to which the article has been submitted; and agreed to be accountable for all aspects of the work.

Funding

This study was supported by the Natural Science Foundation of Jiangsu Province (BK20231120 to X.Z., BK20211005 to J.J.), the Key Research and Development Program of Jiangsu Province of China (BE2020620 to Y.X.), Jiangsu Province Key Medical Discipline (ZDXK202216 to Y.X.), and the Nanjing Medical Science and Technology Development Foundation (ZKX22025 to X.Z.).

Disclosure

The authors declare that they have no known competing financial interests or personal relationships that could influence the work reported in this study.

References

1. GBD 2021 Stroke Risk Factor Collaborators. Global, regional, and national burden of stroke and its risk factors, 1990–2021: a systematic analysis for the Global Burden of Disease Study 2021. *Lancet Neurol*. 2024;23(10):973–1003. doi:10.1016/s1474-4422(24)00369-7
2. GBD 2021 Diseases and Injuries Collaborators. Global incidence, prevalence, years lived with disability (YLDs), disability-adjusted life-years (DALYs), and healthy life expectancy (HALE) for 371 diseases and injuries in 204 countries and territories and 811 subnational locations, 1990–2021: a systematic analysis for the Global Burden of Disease Study 2021. *Lancet*. 2024;403(10440):2133–2161. doi:10.1016/s0140-6736(24)00757-8
3. Pawluk H, Tafelska-Kaczmarek A, Sopońska M, et al. The influence of oxidative stress markers in patients with ischemic stroke. *Biomolecules*. 2024;14(9):1130. doi:10.3390/biom14091130
4. Sato Y, Falcone-Juengert J, Tominaga T, Su H, Liu J. Remodeling of the neurovascular unit following cerebral ischemia and hemorrhage. *Cells*. 2022;11(18):2823. doi:10.3390/cells11182823
5. Qin C, Zhou L-Q, Ma X-T, et al. Dual functions of microglia in ischemic stroke. *Neurosci Bull*. 2019;35(5):921–933. doi:10.1007/s12264-019-00388-3
6. Wang Z, Bai S, Song Y, et al. Impact of NBP on acute ischemic stroke: tracking therapy effect on neuroinflammation. *Int Immunopharmacol*. 2024;143(Pt 1):113217. doi:10.1016/j.intimp.2024.113217
7. Ma Y, Zheng K, Zhao C, et al. Microglia LILRB4 upregulation reduces brain damage after acute ischemic stroke by limiting CD8(+) T cell recruitment. *J Neuroinflammation*. 2024;21(1):214. doi:10.1186/s12974-024-03206-4
8. Li H, Liu P, Zhang B, et al. Acute ischemia induces spatially and transcriptionally distinct microglial subclusters. *Genome Med*. 2023;15(1):109. doi:10.1186/s13073-023-01257-5
9. Lan Z, Qu LJ, Liang Y, et al. AZD1390, an ataxia telangiectasia mutated inhibitor, attenuates microglia-mediated neuroinflammation and ischemic brain injury. *CNS Neurosci Ther*. 2024;30(4):e14696. doi:10.1111/cns.14696
10. Ge JW, Deng SJ, Xue ZW, et al. Imperatorin inhibits mitogen-activated protein kinase and nuclear factor kappa-B signaling pathways and alleviates neuroinflammation in ischemic stroke. *CNS Neurosci Ther*. 2022;28(1):116–125. doi:10.1111/cns.13748
11. Yoon JS, Sung SH, Kim YC. Neuroprotective limonoids of root bark of Dictamnus dasycarpus. *J Nat Prod*. 2008;71(2):208–211. doi:10.1021/np070588o
12. Jeong GS, Byun E, Li B, Lee DS, Kim YC, An RB. Neuroprotective effects of constituents of the root bark of Dictamnus dasycarpus in mouse hippocampal cells. *Arch Pharm Res*. 2010;33(8):1269–1275. doi:10.1007/s12272-010-0818-9
13. Luo X, Yu Z, Yue B, et al. Obacunone reduces inflammatory signalling and tumour occurrence in mice with chronic inflammation-induced colorectal cancer. *Pharm Biol*. 2020;58(1):886–897. doi:10.1080/13880209.2020.1812673
14. Calvo B, Rubio F, Fernández M, Tranque P. Dissociation of neonatal and adult mice brain for simultaneous analysis of microglia, astrocytes and infiltrating lymphocytes by flow cytometry. *IBRO Rep*. 2020;8:36–47. doi:10.1016/j.ibror.2019.12.004
15. Fu Y-J, Xu B, Huang S-W, et al. Baicalin prevents LPS-induced activation of TLR4/NF-κB p65 pathway and inflammation in mice via inhibiting the expression of CD14. *Acta Pharmacol Sin*. 2021;42(1):88–96. doi:10.1038/s41401-020-0411-9
16. Barthels D, Das H. Current advances in ischemic stroke research and therapies. *Biochim Biophys Acta Mol Basis Dis*. 2020;1866(4):165260. doi:10.1016/j.bbadis.2018.09.012
17. Chen L, Zhang R, Xiao J, et al. Neuroprotective effects of eugenol acetate against ischemic stroke. *J Inflamm Res*. 2025;18:133–146. doi:10.2147/jir.S487482
18. Liang Y, Chen L, Huang J, et al. Neuroprotective effects of Aucubin against cerebral ischemia-reperfusion injury. *Int Immunopharmacol*. 2024;129:111648. doi:10.1016/j.intimp.2024.111648
19. Bieber M, Gronewold J, Scharf AC, et al. Validity and reliability of neurological scores in mice exposed to middle cerebral artery occlusion. *Stroke*. 2019;50(10):2875–2882. doi:10.1161/strokeaha.119.026652
20. Sun L, Chen D, Zhao C, et al. Echinatin protects from ischemic brain injury by attenuating NLRP3-related neuroinflammation. *Neurochem Int*. 2024;175:105676. doi:10.1016/j.neuint.2024.105676
21. Yao L, Chen R, Zheng Z, et al. Translational evaluation of metabolic risk factors impacting DBS efficacy for PD-related sleep and depressive disorders: preclinical, prospective and cohort studies. *Int J Surg*. 2025;111(1):543–566. doi:10.1097/js9.0000000000002081

22. Yao L, Lu F, Koc S, et al. LRRK2 Gly2019Ser mutation promotes ER stress via interacting with THBS1/TGF-β1 in Parkinson's disease. *Adv Sci*. 2023;10(30):e2303711. doi:10.1002/advs.202303711
23. He Q, Song F, Wang Y, Chen Z. Mechanistic investigation of Xijiao Dihuang decoction for ischemic stroke: a network pharmacology and in vivo validation study. *Adv Neurol*. 2025;5(1):56–79. doi:10.36922/an025100020
24. Zou X, Gao S, Li J, et al. A monoamine oxidase B inhibitor ethyl ferulate suppresses microglia-mediated neuroinflammation and alleviates ischemic brain injury. *Front Pharmacol*. 2022;13:1004215. doi:10.3389/fphar.2022.1004215
25. Zhang Q, Ran T, Li S, et al. Catalpol ameliorates liver fibrosis via inhibiting aerobic glycolysis by EphA2/FAK/Src signaling pathway. *Phytomedicine*. 2024;135:156047. doi:10.1016/j.phymed.2024.156047
26. Shang J, Wen Y, Zhang X, et al. Naoxintong capsule accelerates mitophagy in cerebral ischemia-reperfusion injury via TP53/PINK1/PRKN pathway based on network pharmacology analysis and experimental validation. *J Ethnopharmacol*. 2025;336:118721. doi:10.1016/j.jep.2024.118721
27. Jafari R, Almqvist H, Axelsson H, et al. The cellular thermal shift assay for evaluating drug target interactions in cells. *Nat Protoc*. 2014;9(9):2100–2122. doi:10.1038/nprot.2014.138
28. Tu Y, Tan L, Tao H, Li Y, Liu H. CETSA and thermal proteome profiling strategies for target identification and drug discovery of natural products. *Phytomedicine*. 2023;116:154862. doi:10.1016/j.phymed.2023.154862
29. Chen P, Wang Y, Tang H, et al. New applications of clioquinol in the treatment of inflammation disease by directly targeting arginine 335 of NLRP3. *J Pharm Anal*. 2025;15(1):101069. doi:10.1016/j.jpha.2024.101069
30. Jayaraj RL, Azimullah S, Beiram R, Jalal FY, Rosenberg GA. Neuroinflammation: friend and foe for ischemic stroke. *J Neuroinflammation*. 2019;16(1):142. doi:10.1186/s12974-019-1516-2
31. Wang M, Li Q, Ren B, et al. Ethanolic extract of Arctium lappa leaves alleviates cerebral ischemia reperfusion-induced inflammatory injury via HDAC9-mediated NF-κB pathway. *Phytomedicine*. 2024;129:155599. doi:10.1016/j.phymed.2024.155599
32. Zhang H, Zhu Y, Zhu G, Yang S. Clinical efficacy and mechanistic insights of Anshen Dingzhi prescription on breast cancer-related PTSD through network pharmacology and molecular docking. *Integr Cancer Ther*. 2024;23:15347354241285435. doi:10.1177/15347354241285435
33. Yuan J, Liang X, Zhou W, et al. TRPA1 promotes cisplatin-induced nephrotoxicity through inflammation mediated by the MAPK/NF-κB signaling pathway. *Ann Transl Med*. 2021;9(20):1578. doi:10.21037/atm-21-5125
34. Satyanarayanan SK, Han Z, Xiao J, et al. Frontiers of neurodegenerative disease treatment: targeting immune cells in brain border regions. *Brain Behav Immun*. 2025;123:483–499. doi:10.1016/j.bbi.2024.10.007
35. Lyu J, Xie D, Bhatia TN, Leak RK, Hu X, Jiang X. Microglial/Macrophage polarization and function in brain injury and repair after stroke. *CNS Neurosci Ther*. 2021;27(5):515–527. doi:10.1111/cns.13620
36. Var SR, Shetty AV, Grande AW, Low WC, Cheeran MC. Microglia and macrophages in neuroprotection, neurogenesis, and emerging therapies for stroke. *Cells*. 2021;10(12):3555. doi:10.3390/cells10123555
37. Zhou Y, Gu J, Li J, et al. Obacunone, a promising phytochemical triterpenoid: research progress on its pharmacological activity and mechanism. *Molecules*. 2024;29(8):1791. doi:10.3390/molecules29081791
38. Li J, Deng SH, Li J, et al. Obacunone alleviates ferroptosis during lipopolysaccharide-induced acute lung injury by upregulating Nrf2-dependent antioxidant responses. *Cell Mol Biol Lett*. 2022;27(1):29. doi:10.1186/s11658-022-00318-8
39. Chen Y, Peng M, Li W, et al. Inhibition of inflammasome activation via sphingolipid pathway in acute lung injury by Huanglian Jiedu decoction: an integrative pharmacology approach. *Phytomedicine*. 2022;107:154469. doi:10.1016/j.phymed.2022.154469
40. Luo X, Yue B, Yu Z, et al. Obacunone protects against ulcerative colitis in mice by modulating gut microbiota, attenuating TLR4/NF-κB signaling cascades, and improving disrupted epithelial barriers. *Front Microbiol*. 2020;11:497. doi:10.3389/fmicb.2020.00497
41. Prabhakaran S, Gonzalez NR, Zachrison KS, et al. 2026 Guideline for the early management of patients with acute ischemic stroke: a guideline from the American Heart Association/American Stroke Association. *Stroke*. 2026. doi:10.1161/str.0000000000000513
42. Bernis ME, Hakvoort C, Nacarkucuk E, et al. Neuroprotective effect of clemastine improved oligodendrocyte proliferation through the MAPK/ERK pathway in a neonatal hypoxia ischemia rat model. *Int J Mol Sci*. 2024;25(15):8204. doi:10.3390/ijms25158204
43. Burguete MC, Jover-Mengual T, Castelló-Ruiz M, et al. Cerebroprotective effect of 17β-Estradiol replacement therapy in ovariectomy-induced post-menopausal rats subjected to ischemic stroke: role of MAPK/ERK1/2 pathway and PI3K-independent Akt activation. *Int J Mol Sci*. 2023;24(18):14303. doi:10.3390/ijms241814303
44. Schanbacher C, Bieber M, Reinders Y, et al. ERK1/2 activity is critical for the outcome of ischemic stroke. *Int J Mol Sci*. 2022;23(2):706. doi:10.3390/ijms23020706
45. Costa C, Quaglio AEV, Di Stasi LC. Pfaffia paniculata (Brazilian ginseng) extract modulates Mapk and mucin pathways in intestinal inflammation. *J Ethnopharmacol*. 2018;213:21–25. doi:10.1016/j.jep.2017.10.009
46. Okazaki R, Doi T, Hayakawa K, et al. The crucial role of Erk2 in demyelinating inflammation in the central nervous system. *J Neuroinflammation*. 2016;13(1):235. doi:10.1186/s12974-016-0690-8
47. Yang L, Tao L-Y, Chen X-P. Roles of NF-κB in central nervous system damage and repair. *Neurosci Bull*. 2007;23(5):307–313. doi:10.1007/s12264-007-0046-6
48. Wang L, Yin C, Liu T, et al. Pellino1 regulates neuropathic pain as well as microglial activation through the regulation of MAPK/NF-κB signaling in the spinal cord. *J Neuroinflammation*. 2020;17(1):83. doi:10.1186/s12974-020-01754-z
49. Jiang Z, Zeng Z, He H, et al. Lycium barbarum glycopeptide alleviates neuroinflammation in spinal cord injury via modulating docosahexaenoic acid to inhibiting MAPKs/NF-kB and pyroptosis pathways. *J Transl Med*. 2023;21(1):770. doi:10.1186/s12967-023-04648-9
50. Peng Z, Li X, Li J, et al. Dlg1 knockout inhibits microglial activation and alleviates lipopolysaccharide-induced depression-like behavior in mice. *Neurosci Bull*. 2021;37(12):1671–1682. doi:10.1007/s12264-021-00765-x
51. Liu Z, Yao X, Sun B, et al. Pretreatment with kaempferol attenuates microglia-mediate neuroinflammation by inhibiting MAPKs-NF-κB signaling pathway and pyroptosis after secondary spinal cord injury. *Free Radic Biol Med*. 2021;168:142–154. doi:10.1016/j.freeradbiomed.2021.03.037
52. Kumar SK, Mani KP. Proinflammatory signaling mechanism of endocan in macrophages: involvement of TLR2 mediated MAPK-NFkB pathways. *Cytokine*. 2024;175:156482. doi:10.1016/j.cyto.2023.156482
53. Lu S, Luo Y, Sun G, Sun X. Ginsenoside compound K attenuates Ox-LDL-mediated macrophage inflammation and foam cell formation via autophagy induction and modulating NF-κB, p38, and JNK MAPK signaling. *Front Pharmacol*. 2020;11:567238. doi:10.3389/fphar.2020.567238